# Directing the Self-Assembly of Block Copolymers into A Metastable Complex Network Phase via A Deep and Rapid Quench

Marcus Müller and De-Wen Sun
*Institut für Theoretische Physik, Friedrich-Hund-Platz 1, 37077 Göttingen, Germany*
(Received 13 August 2013; published 26 December 2013)

The free-energy landscape of self-assembling block copolymer systems is characterized by a multitude of metastable minima. Using particle-based simulations of a soft, coarse-grained model, we explore opportunities to reproducibly direct the spontaneous ordering of these self-assembling systems into a metastable complex network morphology—specifically, Schoen's I-WP periodic minimal surface—starting from a highly unstable state that is generated by a rapid expansion. This process-directed self-assembly provides an alternative to fine-tuning molecular architecture or blending for fabricating complex network structures. Comparing our particle-based simulation results to recently developed free-energy techniques, we critically assess their ability to predict spontaneous formation and highlight the importance of nonequilibrium molecular conformations in the starting state and the local conservation of density.

DOI: 10.1103/PhysRevLett.111.267801 PACS numbers: 61.25.he, 64.75.Yz, 82.35.Jk

The self-assembly of block copolymer materials results in the spontaneous formation of spatially modulated morphologies at the length scale of 10–100 nm. The stability of morphologies of $AB$ diblock copolymers in the bulk is understood in terms of the interfacial tension between different domains and chain stretching [1]. In addition to the known stable morphologies, however, there is a multitude of metastable states [2–4]. In fact, the rugged free-energy landscape of block copolymers has been likened to that of glass-forming systems [5], giving rise to long-lived metastable states.

Network morphologies in block copolymer systems are of particular interest due to their beneficial physical attributes for a variety of technological applications [6,7], ranging from separation membranes for gases [8] or in fuel cells [9], photonic crystals [10,11], to food [12]. Previous effort has focused on making the desired morphology the thermodynamic equilibrium state by fine-tuning molecular architecture or blending [13–15]. In this Letter, we pursue a different strategy. Tailoring the kinetics of structure formation in block copolymers, we propose to reproducibly direct the self-assembly of block copolymers such that the system becomes trapped in the desired long-lived metastable morphology. To this end, it is necessary to (i) control the generation of well-defined, highly unstable states and (ii) design the unstable state such that the ensuing spontaneous kinetics of structure formation reaches the desired metastable morphology.

Highly unstable states of multicomponent polymer systems can be generated in a controlled way because one can change thermodynamic control parameters, e.g., volume or pressure [16,17], on a time scale of milliseconds that is much shorter than the time scale $\tau$ that characterizes the evolution of the fastest growing, spinodal mode of the unstable state [18]. Typically, $\tau = R_{e0}^2/D$, where $R_{e0}$ is the end-to-end distance of the macromolecules and $D$ denotes the self-diffusion coefficient, is comparable to the longest relaxation time of chain conformations and it is on the order of seconds. This characteristic of macromolecular systems allows us to fabricate highly unstable states by rapid and deep quenches. Deep and rapid pressure quenches have been used experimentally, e.g., to investigate the early stages of spinodal phase separation in polymer blends [19,20].

In this Letter we exploit this "process-directed" self-assembly [21–23] to trap the structure formation of a compressible diblock copolymer liquid into a complex network morphology, and we critically assess the ability of recently devised computational techniques—on-the-fly string method [24–26] and its analog for locally conserved order parameters [27]—to predict the kinetics of structure formation after a rapid and deep pressure quench.

We describe the universal aspects of compressible block copolymer materials by a soft, coarse-grained model. Each diblock copolymer is composed of $f_A N = 4$ segments of species $A$ and $(1 - f_A)N = 28$ $B$ segments. This asymmetry results in a stable bcc morphology for symmetric segment volumes and statistical segment lengths according to self-consistent field theory (SCFT). The chain discretization $N = 32$ is chosen as a balance between computational feasibility and accuracy of representing the molecular architecture. The bonded interactions along the Gaussian chains take the form $\mathcal{H}_b/k_BT = \sum_{i,t}(3/2b_t^2)(\mathbf{r}_{i,t} - \mathbf{r}_{i,t-1})^2$, where $\mathbf{r}_{i,t}$ is the coordinate of the $t$th coarse-grained segment of polymer $i$, $b_t$ denotes the statistical segment length of the $t$th bond along the polymer backbone, and the sum over $i$ comprises all $n$ polymers [28,29]. In the following, all lengths of this particle analog of the standard Gaussian chain model [30] are measured in units of the end-to-end distance $R_{e0}$ in the absence of nonbonded interactions.

$A$ and $B$ species repel each other, and there is a large difference in compressibility between $A$ and $B$ domains. For

 

instance, the compressibility of an $A$ domain could be enhanced by selective swelling with a supercritical solvent like carbon dioxide [31–34]. Alternatively, one could envision that the selectivity of the solvent for the two species strongly depends on pressure: In the compressed state, the solvent is uniformly distributed, but, in the expanded state, it is preferentially located in the $A$ domains [35]. We model the equation of state of the compressible binary system by a general, local, nonbonded free-energy functional [36,37] $\mathcal{F}_{\rm nb}/k_BT = \int (d\mathbf{r}/R_{e0}^3) f_{\rm nb}(\hat{\rho}_A, \hat{\rho}_B)$, where $\hat{\rho}_A(\mathbf{r}) \equiv (R_{e0}^3/N)\sum_{i_A}\delta(\mathbf{r}-\mathbf{r}_{i_A})$ is the local $A$ density, $i_A$ runs over all $A$ segments, and $f_{\rm nb} = (v_A/2)\hat{\rho}_A^2 + v_{AB}\hat{\rho}_A\hat{\rho}_B + (v_B/2)\hat{\rho}_B^2 - (w_A/3)\hat{\rho}_A^3 - (w_B/3)\hat{\rho}_B^3 + (u_A/4)\hat{\rho}_A^4 + (u_B/4)\hat{\rho}_B^4$.

The excess pressure, $\Delta p \equiv -(\partial \mathcal{F}_{\rm nb}/\partial V)$, for the pure components is depicted in Fig. 1. The pure $A$ component is supercritical, whereas the pure $B$ component is a melt with a small compressibility. We choose the coefficients such that both segment species have the same molecular density $\rho R_{e0}^3/N = 8192$, compressibility, and statistical segment lengths, $b_A = b_B = R_{e0}/\sqrt{N-1}$, at high pressure. The stable morphology is a bcc morphology of micelles, and SCFT calculations for this compressible model yield an equilibrium periodicity of $L_{\rm bcc} = 2.357R_{e0}$.

The two domains have equal compressibility at high pressure, and we model the rapid change of the thermodynamic control parameter by an affine expansion (stretch), during which the pressure drops [38]. At low pressure, the segmental volume of $A$ is larger than that of the nearly incompressible $B$ segments, such that the volume fractions of both species are comparable. The increased size of the $A$ segments relative to $B$ segments is also accounted for by rescaling the statistical segment lengths to $b_A\sqrt{N-1} = 2R_{e0}$ and $b_B\sqrt{N-1} = \sqrt{8/14}R_{e0}$ [39]. The specific values are chosen such that the low-pressure state resembles a

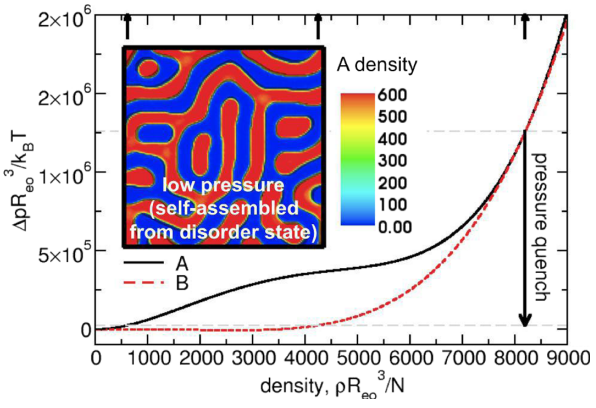


FIG. 1 (color online). Equation of state of the pure $A$ and $B$ domains of the compressible diblock copolymer model. The arrows on top mark the density of $A$ and $B$ segments at low and high pressures. The inset depicts a contour plot of the $A$ density of a system with geometry $R_{e0} \times (10.605R_{e0})^2$ self-assembled from a disordered state at low pressure.

symmetric incompressible diblock copolymer [40]. Spontaneous self-assembly from a disordered morphology yields a lamellar, fingerprint morphology as depicted in the inset of Fig. 1.

The kinetics of structure formation of this soft, coarse-grained model is investigated by single-chain-in-mean-field simulations [28,29,41]. In order to exploit the separation between the strong bonded and weaker nonbonded forces, the nonbonded interactions are temporarily replaced by external fields. The macromolecular conformations are updated by local smart Monte Carlo (MC) moves that mimic diffusive Rouse dynamics and, after 10% of the particles had the chance to move, the external fields are recomputed from the instantaneous, local densities on a collocation grid with spacing $\Delta L \approx R_{e0}/12$.

In the first set of simulations, we equilibrate a large system of dimension $L = 7.07R_{e0}$ at high pressure in the bcc morphology. Then, we affinely scale the particle coordinates to a box size $L = 10.605R_{e0}$ and set the statistical segment lengths to their low-pressure values. Subsequently, we directly observe the kinetics of structure formation starting from this highly unstable bcc morphology. Representative snapshots are presented in Fig. 2.

Immediately after the expansion, the density is approximately uniform, $\rho R_{e0}^3/N = 2427$, whereas the equilibrium densities in the pure $A$ and $B$ domains are 607 and 4248, respectively. Initially, we observe a decrease of the high density inside the $A$ domains and a balancing of the pressure inside the unit cell (i) via expansion of the size of the spherical $A$ domains and (ii) by "evaporating" $A$ blocks into the $B$ matrix. The latter effect is facilitated by the significantly stretched $B$ blocks that pull the short $A$ fragment into the $B$ matrix. The relaxation of the conformational properties after the rapid quench is illustrated in Fig. 3. Both effects result in an increase of the $A$ density inside the $B$ matrix. Subsequently, the excess of $A$ in the $B$ matrix leads to the formation of a new $A$ domain. After about 1000 MC steps the chain configurations equilibrate. Thermal fluctuations result in a network morphology with defects. To illustrate the average structure we fold back the $A$ density into the cubic unit cell (cf. inset of Fig. 2). The average metastable morphology is composed of a continuous $B$ domain and two types of $A$ domains—the spherical $A$ domains of the original bcc structure and new $A$ domains that form inside the original $B$ matrix. The $B$ domain wraps the spherical $A$ domains and bridges between the eight nearest neighbor spheres forming a single eightfold coordinated network; we denote this complex network morphology according to Schoen by I-WP structure. This morphology is a new network phase in addition to gyroid, diamond, and primitive phases [42,43], whose stability in block copolymer systems has previously been discussed in Ref. [44]. This metastable morphology only evolves slowly during simulation runs that extend up to 15000 MC steps, indicating that it is a metastable state. Two additional simulations also resulted in the I-WP morphology; in one of these runs the spherical $A$ domains

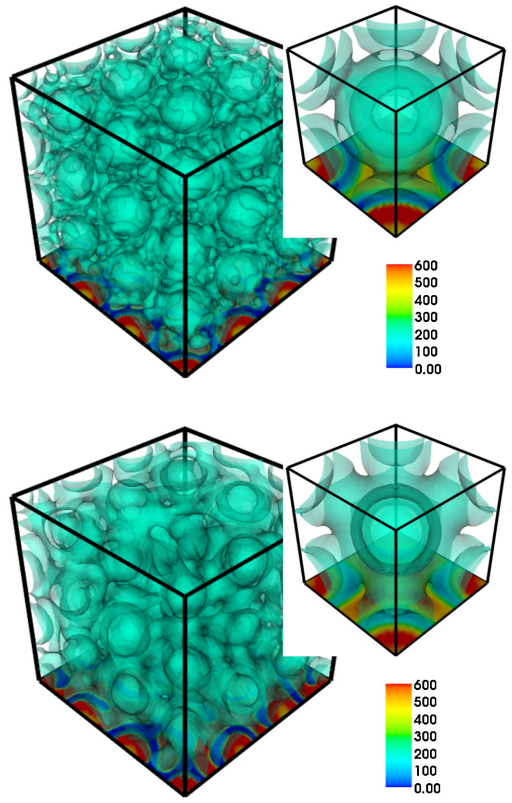


FIG. 2 (color online). Contour plots of the $A$ density at 800 (top) and 15 000 (bottom) MC steps after the rapid pressure quench. The density has been averaged over 100 MC steps. The inset depicts the average morphology of the unit cell depicting the I-WP morphology. The isosurfaces correspond to a density of $\rho_A R_{e0}^3/N = 200$.

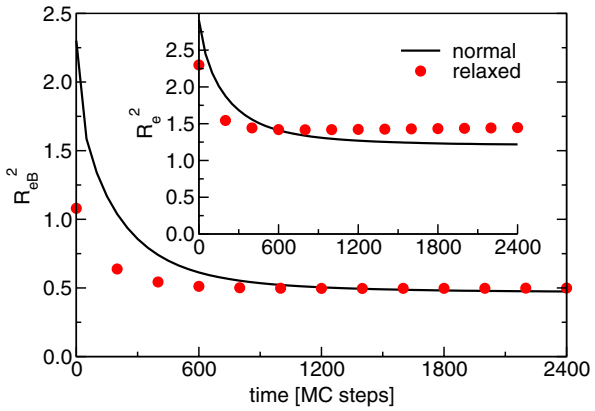


FIG. 3 (color online). Time evolution of the mean-squared end-to-end distance of the $B$ block and the entire block copolymer (inset). The solid line corresponds to the particle-based simulation started from an affinely deformed bcc morphology yielding the I-WP morphology. The circles present the results of the simulation that started from a bcc morphology with relaxed chain conformations yielding an expanded bcc morphology. Statistical errors of the MC data are smaller than the symbol size.

expanded slightly more and the new $A$ domains in the original $B$ matrix were slightly thinner.

In the second set of simulations we have used a field-theoretic umbrella potential $\mathcal{H}_{\text{fup}}/k_BT = \int (d^3\mathbf{r}/R_{e0}^3) \times (\lambda/2)[(\hat{\rho}_A - \phi_A)^2 + (\hat{\rho}_B - \phi_B)^2]$ to restrain fluctuations of the particle densities from the values $\phi_A(\mathbf{r})$ and $\phi_B(\mathbf{r})$ [21,45]. In the limit $\lambda \to \infty$, the partition function $\mathcal{Z}_\lambda$ of this restraint system is related to the free energy $F$ as a functional of the local densities via $F_\lambda[\phi_A, \phi_B] \equiv -k_BT \ln \mathcal{Z}_\lambda \overset{\lambda\to\infty}{\to} F[\phi_A, \phi_B]$. From the averages in the restrained ensemble over 5000 MC steps, we obtain the chemical potential according to $\lambda[\varphi_A(\mathbf{r}) - \langle\hat{\rho}_A(\mathbf{r})\rangle_\lambda] \overset{\lambda\to\infty}{\to} \mu_A(\mathbf{r}) \equiv \delta F/\delta\varphi_A(\mathbf{r})$ and a similar expression holds for $\mu_B(\mathbf{r})$. We use $\lambda = 0.5$ [46].

The numerical knowledge of the chemical potential allows us to compute the minimum free-energy path (MFEP) of the free-energy functional $F[\phi_A, \phi_B]$ via the improved string method [47] without an explicit expression of the free-energy functional $F$ [48]. The MFEP is a sequence of morphologies $\{\phi_{As}(\mathbf{r}), \phi_{Bs}(\mathbf{r})\}$ parametrized by the contour parameter $0 \le s \le 1$ [49] such that the chemical potential perpendicular to the MFEP vanishes, i.e., $\mu_{As}(\mathbf{r}) - (d\varphi_{As}(\mathbf{r})/ds)\,(\int d\mathbf{r} \times \mu_{As}(d\varphi_{As}/ds)/\int d\mathbf{r}(d\varphi_{As}/ds)^2) = 0$ for all points in space and contour parameters, and a similar equation holds for $\mu_B$. The free-energy profile is obtained by integrating the chemical potential along the string.

We obtain the starting point of the string, i.e., the unstable bcc morphology, by minimizing $F$ of the stable high-pressure bcc morphology, thereby eliminating thermal fluctuations, and affinely expanding the morphology from $L = 2.357R_{e0}$ to $3.535R_{e0}$. This starting point, $s = 0$, is fixed. The opposite end, $s = 1$, is the desired network morphology, and its free energy is minimized by the MFEP. We apply periodic boundary conditions and additionally impose mirror symmetry along the 3 cubic axis.

We study the MFEP to the metastable I-WP morphology observed in the simulations as well as to the alternate expanded bcc morphology, where the spherical $A$ domains simply increase their radius and deform. The free energies along the MFEPs from the initial bcc morphology to the metastable structures are presented in Fig. 4. The values of the final metastable structures differ by only a fraction of $k_BT$ per molecule.

The MFEP to the I-WP morphology initially proceeds by increasing the concentration of $A$ throughout the $B$ matrix. Subsequently, this excess amount of $A$ condenses into the percolating $A$ network, and the I-WP morphology is formed. Although the MFEP between the initial bcc morphology and the expanded metastable bcc morphology is initialized by a pointwise spline interpolation, the MFEP does not directly connect the initial bcc structure to the alternate structure but passes through a minimum that resembles the I-WP structure [50]. Thus, the MFEP corroborates the spontaneous conversion of the unstable, initial bcc morphology into the I-WP network structure in agreement with the particle-based simulation of the self-assembly kinetics.

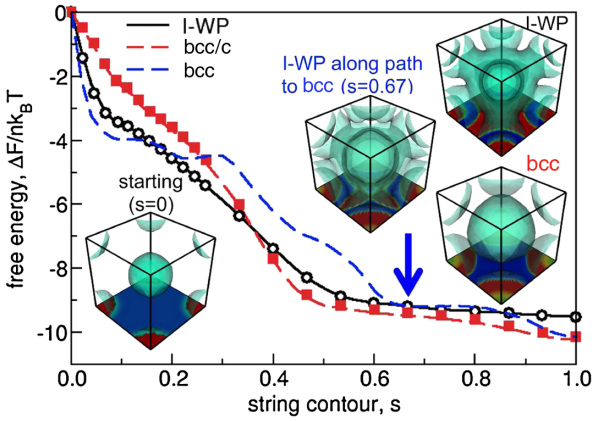


FIG. 4 (color online). MFEP from the unstable bcc morphology to the metastable I-WP network morphology and the conserved transformation path to the expanded bcc state. Snapshots illustrate the initial bcc morphology, the metastable I-WP and expanded bcc morphologies, as well as the metastable I-WP structure along the MFEP towards the expanded bcc morphology at $s = 0.67$.

There are, however, two caveats. (i) The particle-based simulation of the self-assembly kinetics starts from a highly unstable configuration that is not only characterized by its density but additionally by the stretched macromolecular conformations. Since the spontaneous self-assembly occurs on the same time scale as the relaxation of chain conformations, the assumption that the free energy of the system can be described by a functional of the local densities alone warrants study. To highlight the role of conformational stress in the initial state, we have used the field-theoretic umbrella potential to equilibrate the chain conformations keeping the densities of the initial, unstable bcc morphology at $s = 0$ fixed. Starting the unrestrained kinetics of self-assembly from this initial configuration, where the chain conformations are less stretched (cf. Fig. 3), we observe that the spherical $A$ domains simply expand and the I-WP morphology is not formed. Since our MFEP, like SCFT calculations, tacitly assumes that the chain conformations be in equilibrium with the instantaneous values of the density fields, it should rather predict this expanded bcc morphology. (ii) The spontaneous kinetics of self-assembly does not follow the MFEP because the densities are locally conserved, giving rise to Cahn-Hilliard dynamics. Zhang and co-workers [27] account for this local conservation constraint by requiring that the perpendicular component of $\nabla \cdot (\phi_A \nabla \mu_A)$ (rather than of $\mu_A$ itself) vanishes along the transformation path [51], and a similar condition holds for the $B$ species. Indeed, this requirement leads to a transformation path (cf. Fig. 4) that connects the initial and the expanded bcc morphology via a fast expansion of the spherical $A$ domains and a smaller amount of $A$ segments in the $B$ matrix in agreement with the particle-based simulations of the kinetics starting from relaxed chain conformations.

These two additional observations, compiled in Table I, indicate that the initial increase of the $A$ concentration throughout the $B$ matrix is crucial for the formation of the I-WP morphology. In the simulations this effect is aided by the stretched $B$ blocks pulling the short $A$ fragments into the $B$ matrix. Along the MFEP, in turn, the $A$ concentration rises in the $B$ matrix because this nonlocal concentration change reduces the free energy.

TABLE I. Comparison of results of the kinetics of structure formation and the MFEP.

| | Kinetics | MFEP |
|---|---|---|
| Stretched conformations, locally conserved density | I-WP | ··· |
| Relaxed conformations, locally conserved density | bcc | bcc |
| Relaxed conformations, nonconserved densities | ··· | I-WP |

In summary, we have exploited the time-scale separation between the rapid change of a thermodynamic control parameter and the slower unstable modes of structure formation to reproducibly direct the spontaneous kinetics of structure formation from an unstable state such that it becomes trapped in the I-WP morphology [44]. This process-directed self-assembly is a general strategy for fabricating complex morphology in copolymer materials. We hope that it will be tested by experiments yielding processes for reproducibly fabricating metastable morphologies without the need for synthesizing new macromolecular materials or blending existing ones [13,15]. Optimizing the (temporal) control of the thermodynamic parameter (instead of a rapid quench) may further enlarge the kinetic basin of attraction of the desired metastable morphology. The comparison of the particle-based simulations of this process-directed self-assembly with the underlying free-energy landscape as a functional of the local densities demonstrates the importance of the local conservation of density and highlights the role of conformational stress that evolves on the same time scale as the morphology. These findings are independent from the specific model, and the latter indicates a need for devising free-energy functionals that include the conformational stress as slowly relaxing variables [52].

We acknowledge discussions with K. Ch. Daoulas, Y. G. Kevrekidis, L. J. An, and Z. Y. Sun. M. M. thanks T. Qian for pointing him to Ref. [27] and acknowledges hospitality of the Isaac-Newton Institute, Cambridge, UK. Financial support was provided by the DFG Mu1674/9-2 and Mu1674/14-1 and the Volkswagen foundation. Simulations were performed at HLRN Hannover/Berlin and JSC Jülich, Germany.

[1] M. W. Matsen and F. S. Bates, Macromolecules **29**, 1091 (1996).
[2] F. Drolet and G. H. Fredrickson, Phys. Rev. Lett. **83**, 4317 (1999).

[3] Y. Bohbot-Raviv and Z.-G. Wang, Phys. Rev. Lett. **85**, 3428 (2000).
[4] Z. J. Guo, G. J. Zhang, F. Qiu, H. D. Zhang, Y. L. Yang, and A. C. Shi, Phys. Rev. Lett. **101**, 028301 (2008).
[5] C.-Z. Zhang and Z.-G. Wang, Phys. Rev. E **73**, 031804 (2006).
[6] A. J. Meuler, M. A. Hillmyer, and F. S. Bates, Macromolecules **42**, 7221 (2009).
[7] H. Sai, K. W. Tan, K. Hur, E. Asenath-Smith, R. Hovden, Y. Jiang, M. Riccio, D. A. Muller, V. Elser, L. A. Estroff, S. M. Gruner, and U. Wiesner, Science **341**, 530 (2013).
[8] T. A. Shefelbine, M. E. Vigild, M. W. Matsen, D. A. Hajduk, M. A. Hillmyer, E. L. Cussler, and F. S. Bates, J. Am. Chem. Soc. **121**, 8457 (1999).
[9] B. K. Cho, A. Jain, S. M. Gruner, and U. Wiesner, Science **305**, 1598 (2004).
[10] A. M. Urbas, M. Maldovan, P. DeRege, and E. L. Thomas, Adv. Mater. **14**, 1850 (2002).
[11] K. Hur, Y. Francescato, V. Giannini, S. A. Maier, R. G. Hennig, and U. Wiesner, Angew. Chem., Int. Ed. Engl. **50**, 11985 (2011).
[12] R. Mezzenga, W. B. Lee, and G. H. Fredrickson, Trends Food Sci. Technol. **17**, 220 (2006).
[13] M. W. Matsen, Phys. Rev. Lett. **99**, 148304 (2007); , Phys. Rev. Lett. **74**, 4225 (1995).
[14] T. Dotera, Phys. Rev. Lett. **89**, 205502 (2002).
[15] F. J. Martinez-Veracoechea and F. A. Escobedo, Macromolecules **42**, 1775; Macromolecules **42**, 9058 (2009).
[16] B. Rathke, H. Baumgartl, and R. Strey, AIP Conf. Proc. **534**, 414 (2000).
[17] U. Heuert, M. Krumova, G. Hempel, M. Schiewek, and A. Blume, Rev. Sci. Instrum. **81**, 105102 (2010).
[18] F. S. Bates and P. Wiltzius, J. Chem. Phys. **91**, 3258 (1989).
[19] J. Kojima, M. Takenaka, Y. Nakayama, and T. Hashimoto, Macromolecules **32**, 1809 (1999).
[20] M. Takenaka, H. Takeno, T. Hashimoto, and M. Nagao, J. Chem. Phys. **124**, 104904 (2006).
[21] M. Müller and J. J. de Pablo, Annu. Rev. Mater. Sci. **43**, 1 (2013).
[22] The metastability of the hexagonally perforated phase along the MFEP from the lamellar to gyroid morphology has been observed in X. Cheng, L. Lin, W. E, P. Zhang, and A. C. Shi, Phys. Rev. Lett. **104**, 148301 (2010).
[23] T. P. Lodge, Macromol. Chem. Phys. **204**, 265 (2003).
[24] L. Maragliano and E. Vanden-Eijnden, Chem. Phys. Lett. **446**, 182 (2007).
[25] M. Venturoli, E. Vanden-Eijnden, and G. Ciccotti, J. Math. Chem. **45**, 188 (2009).
[26] M. Müller, Y. G. Smirnova, G. Marelli, M. Fuhrmans, and A. C. Shi, Phys. Rev. Lett. **108**, 228103 (2012).
[27] W. Zhang, T. J. Li, and P. W. Zhang, Commun. Math. Sci. **10**, 1105 (2012).
[28] K. C. Daoulas, M. Müller, J. J. de Pablo, P. F. Nealey, and G. D. Smith, Soft Matter **2**, 573 (2006).
[29] M. Müller, J. Stat. Phys. **145**, 967 (2011).
[30] M. W. Matsen, J. Phys. Condens. Matter **14**, R21 (2002).
[31] J. J. Watkins, G. D. Brown, V. S. Ramachandra Rao, M. A. Pollard, and T. P. Russell, Macromolecules **32**, 7737 (1999).
[32] D. L. Tomasko, H. B. Li, D. H. Liu, X. M. Han, M. J. Wingert, L. J. Lee, and K. W. Koelling, Ind. Eng. Chem. Res. **42**, 6431 (2003).
[33] E. Yoshida and A. Mineyama, Colloid Polym. Sci. **290**, 183 (2012).
[34] L. Y. Shi, Z. H. Shen, and X. H. Fan, Macromolecules **44**, 2900 (2011).
[35] In these cases, the coarse-grained $A$ particles represent the polymer segments and the solvent particles.
[36] M. Müller, L. G. MacDowell, P. Müller-Buschbaum, O. Wunnike, and M. Stamm, J. Chem. Phys. **115**, 9960 (2001).
[37] M. Müller, L. G. MacDowell, P. Virnau, and K. Binder, J. Chem. Phys. **117**, 5480 (2002).
[38] This protocol (stretch) will mimic the action of a barostat after switching the control parameter, pressure, from a high to a low value if the relaxation of the morphology is slower than the relaxation of the volume.
[39] The instantaneous scaling of the statistical segment lengths will be justified if the relaxation of the volume during the rapid quench is faster than the single-chain relaxation time $\tau$.
[40] The virial coefficients, $v_A = 0.164\,795$, $v_B = 0.003\,363\,16$, $v_{AB}=0.0625044$, $w_A=3.31215\times10^{-5}$, $w_B=3.56247\times10^{-6}$, $u_A = 2.329\,94\times10^{-9}$, $u_B=7.26258\times10^{-10}$, and statistical segment lengths were chosen such that the pressure jump in the compressible system mimics the alchemical transformation from $f_A=1/8$ to $1/2$ in an incompressible system with equal segmental volumes and statistical segment lengths.
[41] E. W. Edwards, M. P. Stoykovich, M. Müller, H. H. Solak, J. J. de Pablo, and P. F. Nealey, J. Polym. Sci. B **43**, 3444 (2005).
[42] A. H. Schoen, NASA Technical Note No. TN D-5541, 1970 [http://ntrs.nasa.gov/archive/nasa/casi.ntrs.nasa.gov/19700020472_1970020472.pdf].
[43] P. J. F. Gandy, S. Bardhan, A. L. Mackay, and J. Klinowski, Chem. Phys. Lett. **336**, 187 (2001).
[44] G. E. Schröder-Turk, A. Fogden, and S. T. Hyde, Eur. Phys. J. B **59**, 115 (2007).
[45] M. Müller and K. C. Daoulas, Phys. Rev. Lett. **107**, 227801 (2011).
[46] This value is much larger than the other nonbonded interactions but sufficiently small to allow for segment motion and not to upset the approximation involved in the single-chain-in-mean-field simulations [28]. The consequences of a finite value of $\lambda$ could be assessed by a fluctuation analysis [26].
[47] W. E, W. Ren, and E. Vanden-Eijnden, J. Chem. Phys. **126**, 164103 (2007).
[48] I. G. Kevrekidis, C. W. Gear, and G. Hummer, AIChE J. **50**, 1346 (2004).
[49] The distance of morphologies at $s$ and $s'$ is proportional to $\int d\mathbf{r}\{(\phi_{As}-\phi_{As'})^2+(\phi_{Bs}-\phi_{Bs'})^2\}$ and we discretized the path into 24 morphologies. The simulations exceeded $10^6$ MC steps, and the accuracy of the free energy per chain is on the order of $0.5k_BT$.
[50] The saddle point between this I-WP and the bcc morphology is affected by the single unit cell. In a larger system the transition would proceed via nucleation.
[51] Alternatively, this defining condition for the MFEP with conserved order parameter can be derived by considering the transformation from the particle coordinates to the collective densities; cf. L. Maragliano, A. Fischer, E. Vanden-Eijnden, and G. Ciccotti, J. Chem. Phys. **125**, 024106 (2006).
[52] G. H. Fredrickson, J. Chem. Phys. **117**, 6810 (2002).